$$\left(\begin{smallmatrix} \text{M} \\ \text{CS} \end{smallmatrix}\right)$$

Numerical investigation for the GRLW equation using Parabolic Monge Ampere Equation

Abdulghani Ragaa Alharbi

Department of Mathematics
College of Science
Taibah University
Al-Madinah Al-Munawarah, Saudi Arabia

email: arharbi@taibahu.edu.sa

Abstract

In this paper, the numerical solution to the regularized long wave (GRLW) equation is investigated numerically applying two different techniques a Parabolic Monge Ampere (PMA) moving mesh and uniform mesh. The PMA moving mesh is a method for generating a moving mesh which moves as the solution moves with time. The generated mesh is obtained by having the gradient of a grid potential function. I use here the centred finite differences for both schemes. The comparison between these schemes is shown in the last table and figure. The analytical solution is derived in Appendix A. I find a solution when it has only one solitary wave. Next, I show when it has two or three solitary waves. Figures 2D and 3D shows all of these numerical results using the mentioned schemes compared with the exact solution.

1 Introduction

The generalized regularized long wave (GRLW) equation can be written in non-dimensional form as

$$u_t - \mu u_{txx} + p\left(u^{p+1}\right)_x + u_x = 0. \tag{1.1}$$

Here, $u = u(x, t)$ is the amplitude, x is the spatial coordinate and t is time. The dimensionless parameters $p \geq 1$, and μ are positive constants. The GRLW equation Eq. (1.1) is based on the regularized long wave (RLW) equation, taken $p = 1$ in Eq.(1.1), is given by

$$u_t - \mu u_{txx} + p\left(u^2\right)_x + u_x = 0. \tag{1.2}$$

This equation has been employed to model ion acoustic waves in plasmas, longitudinal diffusive waves in elastic rods, pressure waves in liquid gas bubbles, and nonlinear transverse waves in shallow water (the interested reader can be referred to [1] –[15]). Peregrine, Bona and Mahony [1] introduced primarily the RLW equation after that Benjamin [16] essentially derived it from the behavior of long waves in positive x-direction as a model for small amplitude long waves on the surface of the water in a channel. The RLW equation was proposed as an alternative model to the KdV equation by Benjamin [16]. This equation represents the great length of waves and the long waves with opinions of small wave amplitude in numerous physical systems. The RLW equation has been solved in both analytically and numerically by numerous methods, for instance spectral, finite differences, finite element, collocation, and Adomian decomposition techniques. Changna et, al [17] used an adaptive moving mesh finite element to solve the one and two dimensions RLM equation.

Generalizations, for example, the generalized regularized long wave GRLW (which is also defined by the Benjamin-Bona-Mahondy BBM) or the modified regularized long wave (MRLW) equations [18, 19, 20] appear from numerous applications. The MRLW equation, obtained by taking $p = 2$ in Eq. (1.1), is written as

$$u_t - \mu u_{txx} + p\left(u^3\right)_x + u_x = 0. \tag{1.3}$$

This equation was solved by Gardner [21] using B-spline finite element. Khalifa et al. [22] and Karakoc et al. [23] employed finite element methods based on quintic, cubic, and septic collocation for obtaining the numerical solution of the MRLW equation. Raslan and Hassan [24] employed solitary waves for the MRLW equation. Finite differences methods were employed to solve the MRLW equation by Khalifa [25]. Ali [26] solved numerically the MRLW equation utilizing a mesh-free collocation method. The GRLW equation is studied employing numerous methods, Kaya [27], EL-Danaf et al. [28] and Guo et al.

[29] used numerical methods based on the finite difference scheme, element-free KP-Ritz, and decomposition scheme. A Petrov-Galerkin method was employed to the GRLW equation by Roshan [30]. Ramos [31] applied an approximate quasilinearization scheme to solve the GRLW equation with an initial condition on the formation of an undular bore.

The section of numerical results, here, concentrates on solving the GRLW equation using several techniques, the uniform mesh and PMA moving mesh. I follow the PMA moving mesh technique described in [32, 33, 34, 35]. This technique based on the r-adaptive moving mesh method [36, 35, 37], which generates the moving mesh using the gradient potential function. the fundamental part of this technique is the suitable choice of the monitor function which controls the movement of the mesh points so that the region where the solution has, for example, a large variation or curvature. Since the PMA moving mesh technique improves the mesh, the internal layers are resolved more precisely. Also, the PMA moving mesh method can be used in the finite difference techniques. Many applications, for example in fluid mechanics [38, 39], heat transfer [40] and meteorological [33, 34], has been achieved by using a PMA moving mesh techniques.

The purpose of this paper is to focus on implementing the finite difference method on an adaptive moving mesh for solving the one-dimensional GRLW equation; extending this to higher dimensions is currently doing undertaken and will be published elsewhere.

1.1 The GRLW equation and the analytical solution

The GRLW Eq. (1.1) can be written as [30]

$$u_t - \mu u_{txx} + p\left(u^{p+1}\right)_x + u_x = 0, \tag{1.4}$$

where x, t are the spatial and temporal coordinates, respectively. The parameters p, and μ are positive constants. This PDE is considered based on the physical boundary conditions $u \to 0$ and $u_x \to 0$ as $x \to \pm\infty$. The corresponding boundary conditions, on the region $x \in [x_L, x_R]$, are prescribed as

$$u(x_L, t) = u(x_R, t) = 0, \quad u_x(x_L, t) = u_x(x_R, t) = 0, \quad u_{xx}(x_L, t) = u_{xx}(x_R, t) = 0, \quad \forall t \geq 0. \tag{1.5}$$

The analytical solutions (exact solutions) of the GRLW equation, is given by

$$u(x,t) = \left[\rho \; sech^2 \left(\frac{p}{2} \sqrt{\frac{\alpha_0}{\mu(\alpha_0 + 1)}} (x - x_0 - (\alpha_0 + 1)t) \right) \right]^{\frac{1}{p}}, \qquad (1.6)$$

where α_0 is a spread velocity, $\rho = \frac{(p+2)\alpha_0}{2p}$ is an amplitude of the soliton and x_0 is the central location of the initial wave. For further detail, the interested reader can read Appendix 3. This solution obtained also by Gardner et al. [10] and Roshan [30].

2 Numerical results

In this section, I show the numerical results achieved using several techniques a uniform mesh and a PMA moving mesh. In both methods, I use the centred finite difference methods to discretise the spatial derivatives appear in the GRLW equation Eq. (1.1) and keep the derivative of temporal continuous. Hence, the underlying PDE Eq. (1.1) is transferred to a system of ODEs, which I use MATLAB solver (ode15i) to solve.

2.1 Numerical solution of GRLW equation on a fixed mesh

I investigate the numerical solution to Eq. (1.4) using a fixed mesh on the physical domain $[x_L, x_R]$, where is separated into N_x subintervals $[x_i, x_{i+1}]$. The nodes is given to be

$$x_i = (i - 1)\Delta x, \quad \forall x_i \in [x_L, x_R], \quad i = 1, 2, 3, ..., N_x + 1,$$

and $\Delta x = \frac{x_R - x_L}{N_x}$ is uniformly width of per subinterval. I use the finite differences operators to discretise the spatial differentiation appearing in Eq.(1.4) and keep the temporal differentiation continuous. Consequently, a uniform mesh scheme of Eq.(1.4) becomes as follows:

$$\begin{aligned}
(f(u))_t &= -\left(\frac{g_i - g_{i-1}}{\Delta x} \right), \\
f_i &= u_i - \frac{\mu}{\Delta^2 x} (u_{i+1} - 2u_i + u_{i-1}), \\
g_i &= p \, u_{i+1/2}^{p+1} + u_{i+1/2},
\end{aligned} \qquad (2.1)$$

where $i = 1, 2, 3, ..., N_x + 1$, $u_{i+1/2}^{p+1}$ can be evaluated by $u_{i+1/2}^{p+1} = 0.5(u_{i+1}^{p+1} + u_i^{p+1})$ and $u_{i+1/2}$ can also be taken by $u_{i+1/2} = 0.5(u_{i+1} + u_i)$. Subject to the boundary conditions $u_{t,1} = u_{t,N_x+1} = 0$ and the initial condition chosen by the solution of Eq. (1.1) at $t = 0$.
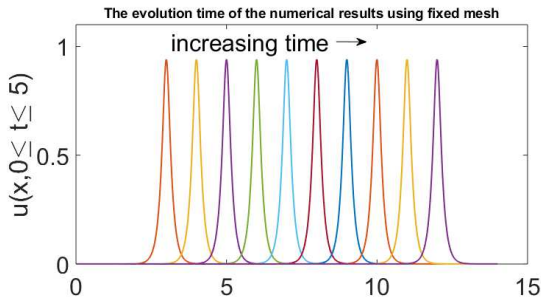

Figure 1: The evolution of time of u of Eq. (1.4) using the fixed mesh scheme, where $t = 0 : 0.5 : 5$. The parameters are taken by $p = 3$, $\mu = 10^{-2}$, $x_0 = 2$, $\alpha_0 = 1.0$ $x_L = 0$, $x_R = 14$ and $N_x = 2000$.

Figure 2.1 illustrated the time evolution of the uniform solution of Eq. (1.4) using the fixed mesh scheme with t is rising among $t = 0$ and $t = 5$, where step temporal here is $\Delta t = 0.5$. The parameters are taken by $p = 3$, $\mu = 10^{-2}$, $x_0 = 2$, $\alpha_0 = 1.0$ $x_L = 0$, $x_R = 14$ and $N_x = 2000$.

2.2 Numerical results on a PMA moving mesh

The fundamental principle that supports the PMA method considered here is to redistribute the mesh points in time as the solution moves with time or adapts to the changes in the solution [32, 33]. The idea of this method is to generate moving mesh nodes by using the gradient of the potential function as the mesh generator [35].

I, here, mostly concentrate on investigating the numerical solution of GRLW Eq. (1.4) applying a PMA moving mesh method. I first continuously map a fixed number of points from the computational domain $[0, 1]$ to the physical domain $[x_L, x_R]$ such that

$$x = x(\xi, t) \colon [0, 1] \to [x_L, x_R], \ t > 0, \tag{2.2}$$

where x and ξ are assumed to be the physical and computational co-ordinates, respectively. Thus, the solution u is given by

$$u(x, t) = u(x(\xi, t), t). \tag{2.3}$$

Hence, the moving mesh is rewritten as

$$x_i(\xi) = x(\xi_i, t), \quad i = 1, \cdots, N_x + 1, \tag{2.4}$$

where $\xi_i = (i-1)/N_x$, $i = 1, \cdots, N_x + 1$. Brenier [41], Caffarelli [42] and Finn [43] proposed that the physical co-ordinate x can also be obtained using the gradient of the mesh potential $P(\xi, t)$. This mesh potential is achieved using the 1D PMA mesh equation, where the 1D PMA mesh equation is given by

$$\tau(1 - \alpha\partial_{\xi\xi})\dot{P} = Q(P_\xi, t)P_{\xi\xi}, \\ x = P_\xi. \tag{2.5}$$

Subject to the boundary condition taken by

$$P_{\xi,1} = x_L, \qquad\qquad P_{\xi,N_x+1} = x_R, \tag{2.6}$$

and initial condition is chosen to be

$$P(\xi_i, t = 0) = 0.5\,\xi_i^2, \qquad\qquad i = 1, 2, \cdots, N_x + 1, \tag{2.7}$$

where $\xi_i \in [0, 1]$ is the computational co-ordinate. Applying the chain rule, yields

$$u_x = \frac{u_\xi}{P_{\xi\xi}}, \qquad u_t = \dot{u} - \frac{u_\xi}{P_{\xi\xi}}\dot{x}. \tag{2.8}$$

Thus, the expression of the GRLW equation Eq. (1.4) is given by

$$\dot{f} - \left(\frac{u_\xi}{P_{\xi\xi}}\right)\dot{P}_\xi + p\left(\frac{u_\xi^{p+1}}{P_{\xi\xi}}\right) + \left(\frac{u_\xi}{P_{\xi\xi}}\right) = 0, \\ f = u - \frac{\mu}{P_{\xi\xi}}\left(\frac{u_\xi}{P_{\xi\xi}}\right)_\xi, \tag{2.9}$$

where $i = 1, ..., N_x$. Subject to the boundary conditions $u_{t,1} = u_{t,N_x+1} = 0$ and the initial condition chosen by the solution of Eq. (1.1) at $t = 0$. Hence, the co-ordinate transformation $x(\xi)$ is obtained by utilizing the 1D PMA mesh equation is given by ([33, 54, 47]):

$$\text{1DPMA}: \quad \dot{P} - \frac{\alpha}{\Delta\xi^2}(\dot{P}_i{+}1{-}2\dot{P}_i{+}\dot{P}_{i-1}) = \frac{1}{\tau}Q(P_\xi, t)\frac{1}{\Delta\xi^2}(P_i{+}1{-}2P_i{+}P_{i-1}), \tag{2.10}$$

where $\Delta\xi$ is the step size of the computational co-ordinate, $Q(P_\xi, t)$ is so-called the monitor function and τ, α are constants. The boundary conditions

are given by $\dot{Q}_1 = 0$ and $\dot{Q}_{N_x+1} = 0$, and the initial condition is taken by Eq. (2.7). Here, I apply the modified arc-length monitor function is proposed by [44, 45, 46, 47]. The modified arc-length monitor function is defined by

$$\text{Arc-length monitor function}: \quad Q(x,t) = \sqrt{b + \lambda \left(\frac{u_\xi}{P_{\xi\xi}}\right)^2}, \qquad (2.11)$$

where λ, b are considered to be non-negative constants. If $lambda = 1$, and $b = 1$, Eq. (2.11) indicates the arc-length monitor function. Several forms of smoothing to the mesh density function are used so as to support the uniform grid [38, 40, 55]. Cook [47] proposed, in 1D, a 3-point smoothing of the monitor function to avoid a sudden change in the regions where the solution has large variations. The smoothed monitor function is defined by

$$\begin{aligned}
\hat{Q} &= \frac{1}{\beta_{-1} + \beta_0 + \beta_1} \left(\beta_{-1} Q_{i-1} + \beta_0 Q_i + \beta_1 Q_{i+1}\right), \\
\hat{Q}_1 &= \frac{1}{\beta_0 + \beta_1} \left(\beta_0 Q_1 + \beta_1 Q_2\right), \\
\hat{Q}_{N_x+1} &= \frac{1}{\beta_{-1} + \beta_0} \left(\beta_{-1} Q_{N_x} + \beta_0 Q_{N_x+1}\right),
\end{aligned} \qquad (2.12)$$

where β_{-1}, β_0, β_1 are the smoothing stencils. Here, I take the stencils by $\beta_{-1} = 1$, $\beta_0 = 2$, $\beta_1 = 1$.

Discretisation

The computational co-ordinate ξ, in this problem, is determined by

$$\xi_i = x_L + (i-1)\Delta\xi, \qquad i = 1, 2, \cdots, N_x + 1, \qquad (2.13)$$

where $\Delta\xi = (x_R - x_L)/N_x$. Then, the physical coordinate x is defined by $x_i = x(\xi_i, t)$, where the boundary grids are forced to be $x_1 = x_L$ and $x_{N_x+1} = x_R$. Thus, the location of the grids x_i is determined as follows

$$x_i = \frac{1}{2\Delta\xi}(P_{i+1}P_{i-1}), \qquad i = 2, \cdots, N_x, \qquad (2.14)$$

where $P_i = P(\xi_i, t)$ is the mesh potential obtained by solving Eq. (2.10). Hence, the semi-discretisation of Eq. (2.9) is defined by

$$\dot{f}_i - \left(\frac{u_{i+1} - u_{i-1}}{P_{i+2} - 2P_i + P_{i-2}} \right) \left(\dot{P}_{i+1} - \dot{P}_{i-1} \right) = 2\Delta\xi \left[p \frac{-(u_{i+1}^{p+1} - u_{i-1}^{p+1})}{P_{i+2} - 2P_i + P_{i-2}} - \frac{u_{i+1} - u_{i-1}}{P_{i+2} - 2P_i + P_{i-2}} \right],$$

$$f_i = u_i - \frac{8\mu\,\Delta\xi^2}{P_{i+2} - 2P_i + P_{i-2}} \left(\frac{u_{i+1} - u_i}{P_{i+2} - P_{i+1} - P_i + P_{i-1}} - \frac{u_i - u_{i-1}}{P_{i+1} - P_i - P_{i-1} + P_{i-2}} \right),$$

$$(2.15)$$

where $i = 3, 4, ..., N_x - 1$.

$$\text{Arc-length monitor function}: \quad Q(x,t) = \sqrt{b + \lambda \left(\frac{2\Delta\xi(u_{i+1} - u_{i-1})}{P_{i+2} - 2P_i + P_{i-2}} \right)^2},$$

$$(2.16)$$

Finally, I study the convergence and the accuracy of both the uniform and the PMA moving mesh schemes. I require to obtain the numerical solutions for both the uniform and the PMA mesh schemes at a fixed time $t = 5$ and compare them with the solution of the exact solution at the same time.

Figures 2 (a, b) present the numerical solution to Eq (2.9) obtained using a PMA moving mesh method with the arc-length monitor function, with parameter values $p = 3$, $\mu = 10^{-2}$, $x_0 = 2$, $\alpha_0 = 1.0$,$\tau = 10^{-3}$, $b = 1$, $\gamma = 5$ and $N_x = 1000$. Time increased among $t = 0$ and $t = 5$ with a temporal step size $\Delta t = 0.5$. Figure 2 (a), at $t = 5$, shows the numerical solution and exact solution evaluated using Eq. (1.1). Notice that the numerical solution is almost the same as the exact solution.

The interaction of two or three solitary waves

If the analytical solution has interaction of more than one solitary wave, it forms as

$$u(x,t) = \sum_{i=1}^{n} \left[\frac{(p+2)\alpha_i}{2p} \; sech^2 \left(\frac{p}{2} \sqrt{\frac{\alpha_i}{\mu(\alpha_i + 1)}} (x - x_i - (\alpha_i + 1)t) \right) \right]^{\frac{1}{p}},$$

$$(2.17)$$

where $n = 2$ or 3.

Table 1 presents the L_2 norm error and CPU time taken to arrive $t = 5$ for both the fixed mesh Eq. (2.1) and the PMA uniform schemes Eq. (2.15)
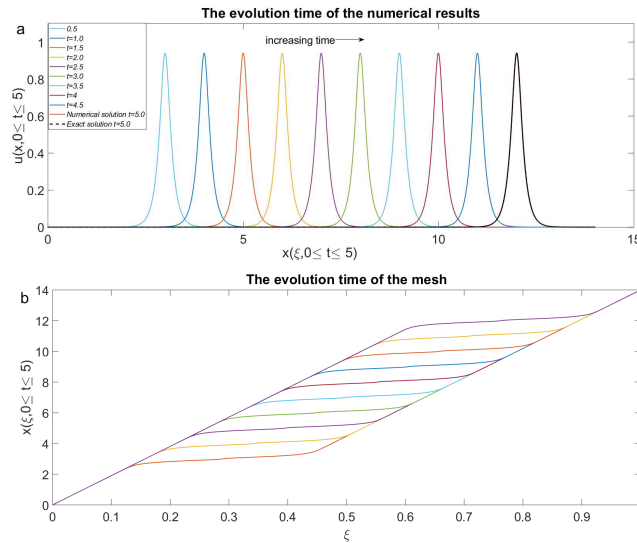
Figure 2: (*a*) Presenting the numerical solution u travelling with time, (*b*) showing the associated mesh obtained employing PMA mesh equation Eq.(2.10) with the arc-length monitor function. Here, the parameter values are taken to be $p = 3$, $\mu = 10^{-2}$, $x_0 = 2$, $\alpha_0 = 1.0$, $\tau = 10^{-3}$, $b = 1$, $\gamma = 5$, $N_x = 1000$ and $t = 0 \rightarrow 5$.

Δx	Uniform mesh scheme		PMA moving mesh	
	Error	CPU	Error	CPU
1	6×10^{-2}	2.3×10^{-1}	9.5×10^{-3}	5×10^{-1} s
0.1	2.2×10^{-4}	2.6×10^{-1}	2×10^{-6}	5.3×10^{-1} s
0.05	5.7×10^{-5}	5×10^{-1}s	1.3×10^{-7}	1.04s
0.02	1.21×10^{-5}	1.42s	7.8×10^{-9}	3.28s
0.01	5.78×10^{-6}	7.97s	4.69×10^{-9}	9.21s
0.005	4.19×10^{-6}	40.2s	4.6×10^{-9}	31s

Table 1: Presenting the L_2 norm error and CPU time taken for both the uniform mesh and PMA moving mesh schemes. The results obtained at $t = 5$ with varying Δx. I evaluated the exact solution Eq. (1.1) at $t = 5$ to measure the errors. The parameters are given by $p = 3$, $alpha_0 = 1.2$, $\mu = 1$, $x_0 = 15$, $b = 1$ and $\lambda = 5$.
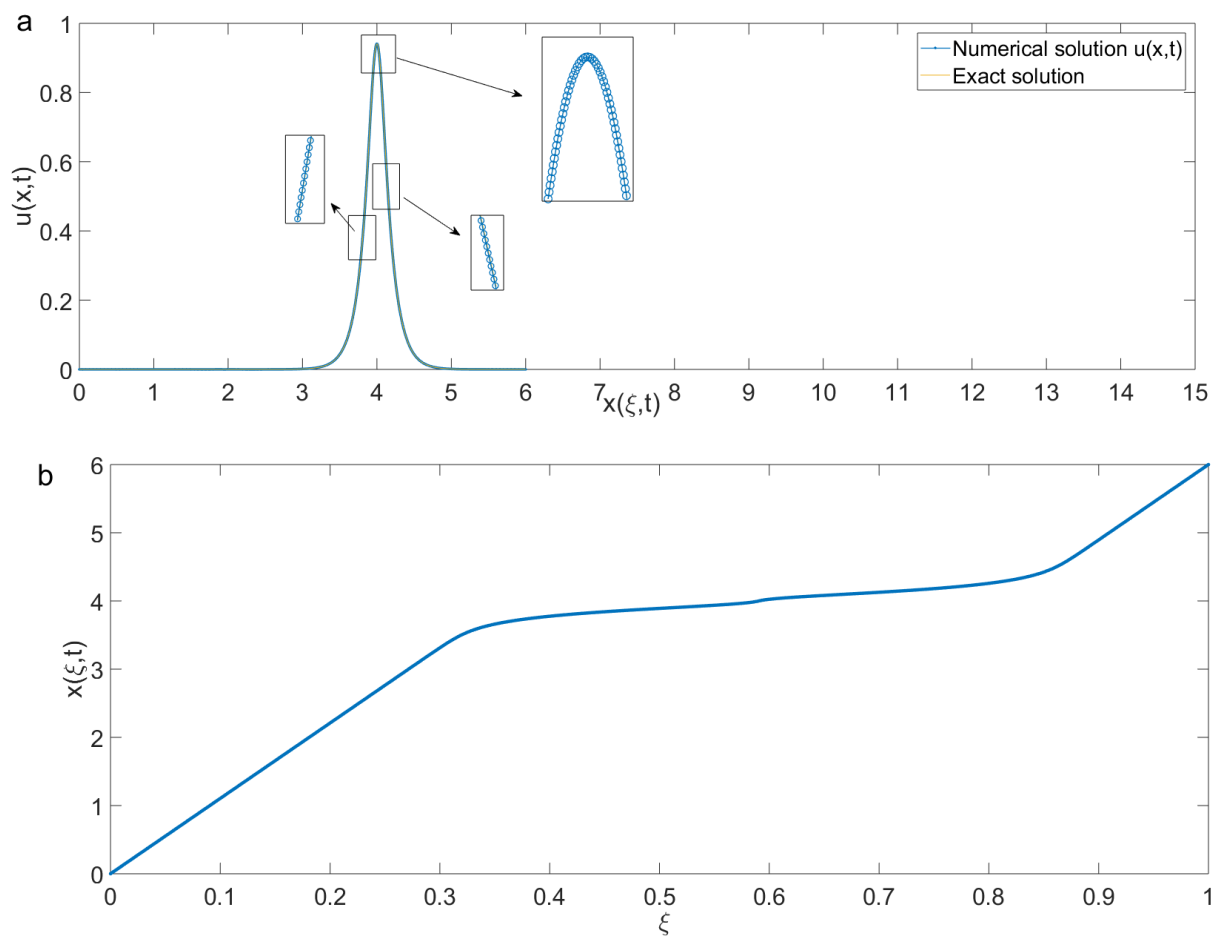
Figure 3: (a) The numerical solution and the exact solution of GRLW equation at $t = 1$ and $N_x = 500$, (b) the associated adaptive mesh $x(\xi, t)$. The PMA mesh scheme is used with the arc-length monitor function with $p = 3$, $\mu = 10^{-2}$, $x_0 = 2$ and $\alpha_0 = 1.0$, $b = 1$ and $\lambda = 5$.
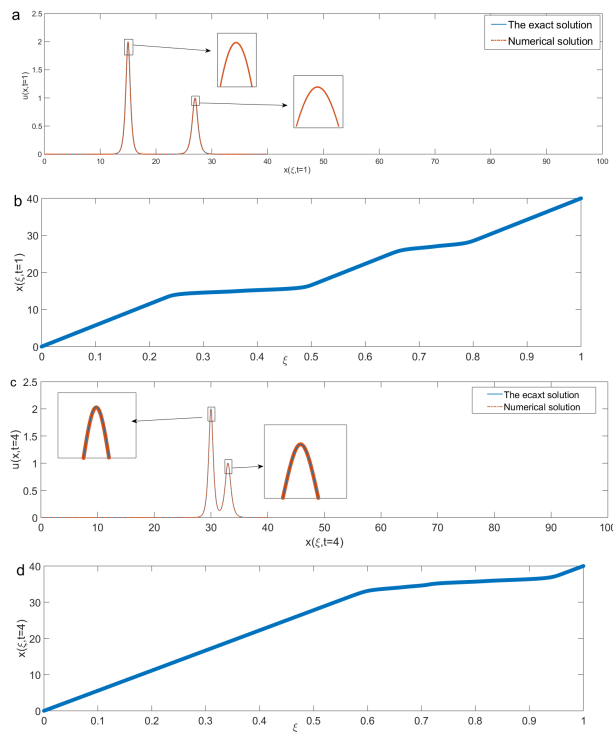
Figure 4: (a, c) Two solitary waves evaluated using the PMA moving mesh scheme with $p = 2$, $\mu = 10^{-1}$, $x_0 = 10$, $x_1 = 25$, $\alpha_0 = 4.0$, $\alpha_1 = 1.0$, $b = 1$, $\tau = 10^{-3}$ and $\lambda = 5$ and $N_x = 4000$ at $t = 1, 4$, respectively. (b, d) the associated adaptive meshes obtained using Eq. (2.10) with the arc-length monitor function at $t = 1, 4$, respectively.
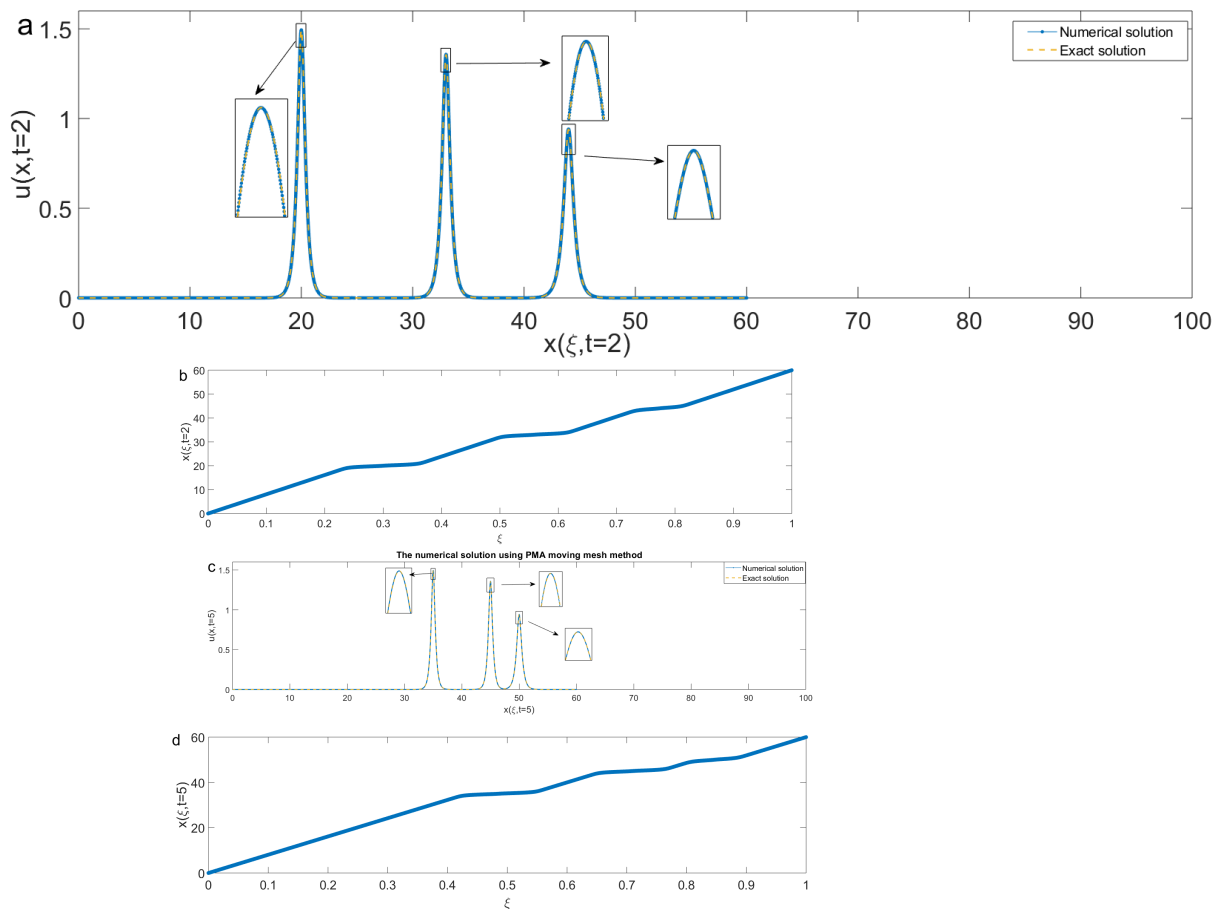
Figure 5: (a) Presenting the three solitary waves evaluated using the PMA moving mesh scheme with $p = 3$, $\mu = 10^{-1}$, $\alpha_0 = 4.0$, $\alpha_1 = 3.0$, $\alpha_2 = 1.0$, $x_0 = 10$, $x_1 = 25$, $x_2 = 40$, $b = 1$, $\tau = 10^{-3}$ and $\lambda = 5$ and $N_x = 4000$ at $t = 2, 5$, respectively. (b, d) the associated adaptive meshes obtained using Eq. (2.10) with the arc-length monitor function at $t = 2, 5$, respectively.
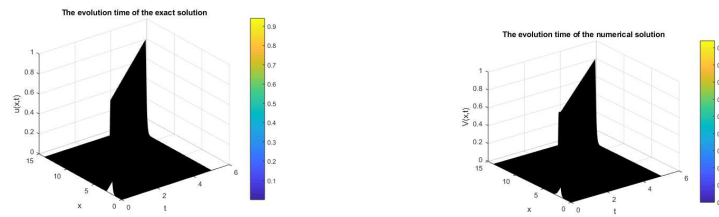
Figure 6: The 3D figures for one solitary wave of both the exact solution investigated Eq. (1.1) and the numerical solution obtained using the PMA moving mesh method. The parameters values are $p = 3$, $\mu = 10^{-2}$, $x_0 = 2$ and $\alpha_0 = 1.0$, $b = 1$ and $\lambda = 5$.
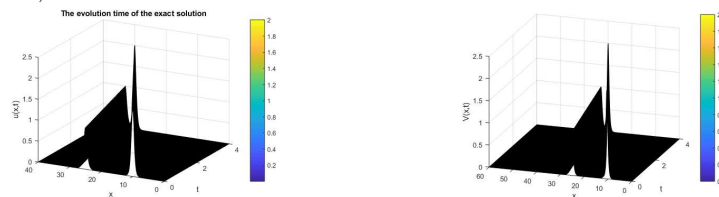

Figure 7: The 3D figures for two solitary waves of both the exact solution investigated Eq. (2.17), $n = 2$, and the numerical solution obtained using the PMA moving mesh method. The parameters values are $p = 2$, $\mu = 10^{-1}$, $x_0 = 10$, $x_1 = 25$, $\alpha_0 = 4.0$, $\alpha_1 = 1.0$, $b = 1$, $\tau = 10^{-3}$ and $\lambda = 5$.
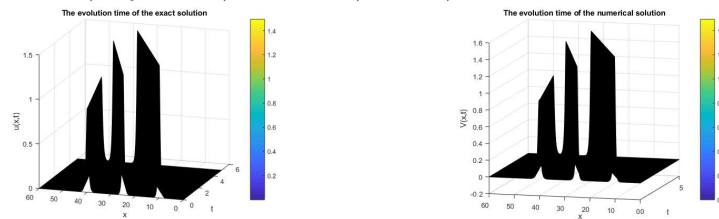

Figure 8: The 3D figures for three solitary waves of both the exact solution investigated Eq. (2.17), $n = 3$, and the numerical solution obtained using the PMA moving mesh method. The parameters values are $p = 3$, $\mu = 10^{-1}$, $\alpha_0 = 4.0$, $\alpha_1 = 3.0$, $\alpha_2 = 1.0$, $x_0 = 10$, $x_1 = 25$, $x_2 = 40$, $b = 1$, $\tau = 10^{-3}$ and $\lambda = 5$.
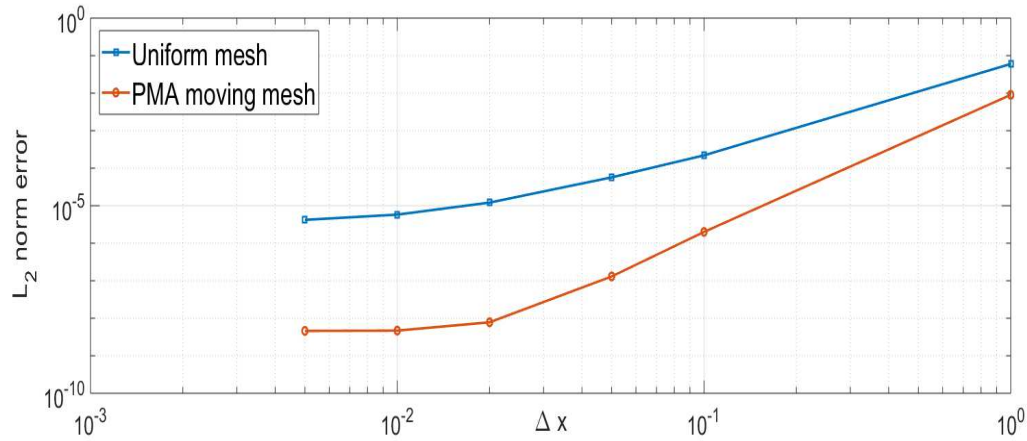
Figure 9: The L_2 error for both the uniform (solid blue line) and PMA moving mesh (solid red) schemes compared with the exact solution evaluated by Eq. (1.1) at $t = 5$ and Δx decreased between 1 and 0.005.

at $t = 5$ with varying Δx. To measure the errors, I compared the numerical results with the exact solution which is evaluated by Eq. (1.1) at the same t and Δx decreased between 1 and 5×10^{-3}. Observe that, from figure 9 the error recorded using a PMA moving mesh scheme is much smaller than the error measured using a uniform mesh. This indicates that the PMA moving mesh scheme is more accurate and convergent than the uniform mesh scheme. It is clear that the lowest error measure is roughly $10-9$ for the PMA moving mesh method at $\Delta x = 0.005$ while the lowest value of the error for the uniform mesh scheme is approximately 10^{-6} to the same Δx. Remark that the lowest error measured for the uniform mesh scheme is about 4×10^{-6} for $\Delta x = 0.005$. The PMA mesh scheme requires $\Delta x = 0.1$ to reach approximately the same error.

3   Conclusions

In this article, I have derived the analytical solution (see Appendix 3. I present some techniques for investigating the numerical results such as a PMA moving mesh and finite difference methods. Actually, I test both of these methods when the solution has interaction of one, two or three solitary waves. All of the numerical results that I present here in figures and table appear the PMA moving mesh method is powerful and accurate.

Appendix

An analytical solution to the GRLW equation Eq. (1.1) is sought here starting with

$$\eta = x - \alpha t, \quad u(x,t) = u(\eta). \tag{3.1}$$

Thus, the GRLW equation Eq. (1.1) is given by

$$(1 - \alpha)u_\eta + \alpha\mu u_{\eta\eta\eta} + p(u^{p+1})_\eta = 0, \tag{3.2}$$

subject to $u \to 0$, $u_\eta \to 0$ as $\eta \to \pm\infty$. Integrating twice with respect to η, leads to

$$(1 - \alpha)u^2 + \alpha\mu u_\eta^2 + \delta u^{p+2} = C_1 u + C_2, \tag{3.3}$$

where C_1 and C_2 are constants and $\delta = \frac{2p}{p+2}$. Using the boundary conditions, yields C_1, $C_2 \to 0$, and then

$$(1 - \alpha)u^2 + \alpha\mu u_\eta^2 + \delta u^{p+2} = 0. \tag{3.4}$$

Using special substitution and integrating both sides with respect to η, leads to

$$u^p = \frac{\alpha}{\delta} sech^2\theta, \tag{3.5}$$

where $\delta = \frac{2p}{p+2}$ and $\theta = \frac{p}{2}\sqrt{\frac{\alpha}{\mu(\alpha+1)}}(x - x_0 - (\alpha + 1)t)$. Thus the exact solution of Eq. (1.1) is given by

$$u(x,t) = \left[\frac{(p+2)\alpha}{2p} sech^2\left(\frac{p}{2}\sqrt{\frac{\alpha}{\mu(\alpha + 1)}}(x - x_0 - (\alpha + 1)t)\right)\right]^{\frac{1}{p}}, \tag{3.6}$$

where x_0 is a constant. Therefore, selecting $p = 2$ in Eq. (3.6) provides the exact solution of MRLW equation Eq. (1.3) and $p = 1$ gives the solution of RLW equation Eq. (1.2).

References

[1] D. H. Peregrine, Calculations of the development of an undular bore, J. Flu. Mech., **25,** no. 2, (1966), 321–330.

[2] J. C. Eilbeck and G. R. McGuire, Numerical study of the regularized long-wave equation I: Numerical methods, J. Comput. Phys., **19,** (1975), 43–57.

[3] J. L. Bona and P. J. Pyrant, A mathematical model for long wave generated by wave makers in nonlinear dispersive systems, Proc. Comp. Philos. Soc., **73,** no. 2, (1973), 391–405.

[4] J. L. Bona, W. G. Pritchard, L. R. Scott, Numerical scheme for a model of nonlinear dispersive waves, J. Comput. Phys., **60,** (1985), 167-176.

[5] M. E. Alexander, J. H. Morris, Galerkin method for some model equation for nonlinear dispersive waves, J. Comput. Phys., **30,** (1979), 428-451.

[6] D. J. Evans, K. R. Raslan, The Tanh function method for solving some important nonlinear partial differential equations, Int. J., **82,** no. 7, (2005), 897-905.

[7] P. C. Jain, R. Shankar, T. V. Single, Numerical solutions of RLW equation, Commun. Numer. Meth. Eng., **9,** (1993), 587-594.

[8] D. Bhardwaj, R. Shankar , A computational method for regularized long wave equation, Comput. Math. Appl., **40,** (2000), 1397-1404.

[9] S. I. Zaki, Solitary waves of the spitted RLW equation, Comput. Phys. Commun., **138,** (2001), 80-91.

[10] L. R. T. Gardner, G. A. Gardner, A. Dogan, A least squares finite element scheme for the RLW equation, Commun. Numer. Meth. Eng., **12,** (1996), 795-804.

[11] I. Dag, Least squares quadratic B-splines finite element method for the regularized long wave equation, Comput. Meth. Appl. Mech. Eng., **182,** (2000), 205-215.

[12] A. A. Soliman, K. R. Raslan, Collocation method using quadratic B-spline for the RLW equation, Int. J. Comput. Math., **78,** (2001), 399-412.

[13] I. Dag, B. Saka, D. Irk, Application of cubic B-splins for numerical solution of the RLW equation, Appl. Math Comput., **195,** (2004), 373-389.

[14] K. R. Raslan, A computational method for the regularized long wave (RLW) equation, Appl. Math. Comput., **176,** (2005), 1101-1118.

[15] A. A. Soliman, M. H. Hussien, Collocation solution for RLW equation with septic splines, Appl. Math. Comput., **161,** (2005), 623-636.

[16] T. B. Benjamin, J. L. Bona, J. J. Mahony, Model equations for long waves in nonlinear dispersive systems, Phil. Trans. Royal Soc. London, Series A, **272,** (1972), 47–78.

[17] C. Lu, W. Huang, J. Qiu, An Adaptive Moving Mesh Finite Element Solution of the Regularized Long Wave Equation, J. Sci. comput., **74,** (2018), 122–144.

[18] J. Avrin, J. A. Goldstein, Global existence for the Benjamin-Bona-Mahony equation in arbitrary dimensions, Nonlinear Anal., **9,** (1985), 861–865.

[19] B. Calvert, The equation $A(t, u(t))' + B(t, u(t)) = 0$, Math. Proc. Cambridge Philos. Soc., **79,** (1976), 545–561.

[20] J. A. Goldstein, B. J. Wichnoski, On the Benjamin-Bona-Mahony equation in higher dimensions, Nonlinear Anal., **4,** (1980), 665–675.

[21] L. R .T. Gardner, G. A. Gardner, F. A. Ayoub, N. K. Amein, Approximations of solitary waves of the MRLW equation by B-spline finite element, Arab. J. Sci. Eng., **22,** (1997), 183-193.

[22] A. K. Khalifa, K.R. Raslan, H. M. Alzubaidi, A finite difference scheme for the MRLW and solitary wave interactions Applied Mathematics and Computation, **189,** (2007), 346-354.

[23] S. B. G. Karakoc, T. Ak, H. Zeybek, An efficient approach to numerical study of the MRLW equation with B-spline collocation method. Abs. App. Anal., (2014), 1-15.

[24] K. R. Raslan, S. M. Hassan, Solitary waves for the MRLW equation, Applied Mathematics Letters, **22,** (2009), 984–989.

[25] A. K. Khalifa, K. R. Raslan, H. M. Alzubaidi, A finite difference scheme for the MRLW and solitary wave interactions, Applied Mathematics and Computation, **189,** (2007), 346-354.

[26] A. Ali, Mesh free collocation method for numerical solution of initial-boundary value problems using radial basis functions, Ghulam Ishaq Khan Institute of Engineering Sciences and Technology, Pakistan, (2009), (Ph.D. thesis).

[27] D. Kaya, A numerical simulation of solitary wave solutions of the generalized regularized long wave equation, Appl. Math.Comput., **149,** (2004), 833-841.

[28] T. S. El Danaf, K. R. Raslan, K. K. Ali, New numerical treatment for the generalized regularized long wave equation based on finite difference Scheme, IJSCE, **4,** no. 4, (2014), 16–24.

[29] B. Y. Guo, W. M. Cao, The fourier pseudospectral method with a restrain operator for the RLW equation, J. Comput. Phys., **74,** (1988), 110–126.

[30] T. Roshan, A petrov-Galerkin method for solving the generalized regularized long wave(GRLW) equation, Appl.Math.Comput., **63,** (2012), 943–956.

[31] J. I. Ramos, Solitary wave interactions of the GRLW equation, Cha. Soli. Fract., **33,** (2007), 479–491.

[32] C. J. Budd, J. F. Williams, Moving mesh generation using the Parabolic MongeAmpre Equation, SIAM J. Sci. comput., **31,** (2009), 3438–3465.

[33] E. Walsh, Moving mesh methods for problems in meteorology, University of Bath, (2010), (Ph. D thesis).

[34] C. J. Budd, M. J. P. Cullen, E. J. Walsh, Monge-Ampère based moving mesh methods for numerical weather prediction, with applications to the Eady problem, J. Comput. Phys., **236,** (2013), 247–270.

[35] C.J. Budd, W. Huang, R. D. Russell, Adaptivity with moving grids, Acta Numerica, **18,** (2009), 111–241.

[36] W. Huang, R. D. Russell, The Adaptive Moving Mesh Methods, Springer, 2011.

[37] V. D. Liseikin, Grid Generation Methods, Springer: New York, NY, USA, 2009.

[38] T. Tang, Moving mesh methods for computational fluid dynamics, Contemporary Mathematics, **383,** (2005), 141–173.

[39] L. Yibao, D. Jeong, J. Kim, Adaptive mesh refinement for simulation of thin film flows, Meccanica, **49,** (2014), 239–252.

[40] H. D. Ceniceros, T. Y. Hou, An Efficient Dynamically Adaptive Mesh for Potentially Singular Solutions, J. Comput. Phys., **172,** no. 2,(2001), 609–639.

[41] Y. Brenier, Polar factorization and monotone rearrangement of vector-valued functions, Commun. Pure App. Math.,**44,** (1991), 375–417.

[42] L. Caffarelli, Interior w 2, p estimates for solutions of the monge-ampere equation, Annals Math., **131,** (1990), 135–150.

[43] J. Finn, G. Delzanno, L. Chacon, Grid generation and adaptation by monge-kantorovich optimization in two and three dimensions, Proceedings of the 17th International Meshing Roundtable, (2008), 551–568.

[44] R. D. Russell, W. Huang, Y. Ren, Moving Mesh Partial Differential Equations (MMPDES) Based on the Equidistribution Principle, Siam. J. Numer. Anal., **31,** (1994), 709–730.

[45] Z. R. Zhang, T. Tang, An adaptive mesh redistribution algorithm for convection-dominated problems, Commun., Pure Appl. Anal., **1,** (2002), 341–357.

[46] J. M. Stockie, J. A. Mackenzie, R. D. Russell, A moving mesh method for one-dimensional hyperbolic conservation laws, SIAM J. Sci. Comput. , **22,** (2000), 1791–1813.

[47] S. P. Cook, Adaptive Mesh Methods for Numerical Weather Prediction, University of Bath, (2016), (Ph.D thesis).

[48] S. Liu, Z. Fu, S. Liu, Q. Zhao, Jacobi elliptic function expansion method and periodic wave solutions of nonlinear wave equations, Phys. Lett., A 289, (2001), 69–74.

[49] Z. Fu, S. Liu, Q. Zhao, New Jacobi elliptic function expansion and new periodic solutions of nonlinear wave equations, Phys. Lett., A 290. (2001), 72–76.

[50] E. Fan, J. Zhang, Applications of the Jacobi elliptic function method to special-type nonlinear equations, Phys. Lett. A 305 (2002), 383–392.

[51] Z. Yan, Abundant families of Jacobi elliptic function solutions of the (2+1)-dimensional integrable DaveyStewartson-type equation via a new method, Chaos Solitons Fractals, **18,** (2003), 299–309.

[52] A. R. Alharbi, S. Naire, An adaptive moving mesh method for thin film flow equations with surface tension, J. Comput. Appl. Math., **319,** no. 4, (2017), 365–384.

[53] A. R. Alharbi, N. Shailesh, An adaptive moving mesh method for two-dimensional thin film flow equations with surface tension, J. Comput. Appl. Math., **356,** (2019), 219–230.

[54] A. R. Alharbi, Numerical solution of thin-film flow equations using adaptive moving mesh methods, Keele University, (2016), (Ph.D thesis).

[55] W. Huang, Practical aspects of formulation and solution of moving mesh partial differential equations, J. of Comp. Phys., **171,** (2001), 753–775.